A quantum moleculardynamics study of protontransfer reactions along asymmetrical H bonds in solution

H. Azzouz and D. Borgis

Citation: J. Chem. Phys. **98**, 7361 (1993); doi: 10.1063/1.464727
View online: http://dx.doi.org/10.1063/1.464727
View Table of Contents: http://jcp.aip.org/resource/1/JCPSA6/v98/i9
Published by the American Institute of Physics.

A quantum molecular-dynamics study of proton-transfer reactions along asymmetrical H bonds in solution

H. Azzouz and D. Borgis[a)]
Laboratoire de Physique Théorique des Liquides, Université Pierre et Marie Curie, 4, Place Jussieu 75252 Paris Cedex 05, France

(Received 2 November 1992; accepted 20 January 1993)

A molecular-dynamics study of a model for $AH-B \rightleftharpoons A^- - H^+ B$ reactions in liquid chloromethane is presented. The parameters of the model are fitted to those of typical OH–N proton-transfer complexes. The rate constant is computed at a quantum level for complexes of various H-bond strength and A-B equilibrium distance. The influence of the properties of the complex on the proton-transfer mechanism is outlined. Also the static and dynamical role of the solvent, the tunneling contribution to the rate, and the associated kinetic isotope effect are discussed. The rate calculations are based on two independent methods. First a curve-crossing, transition-state rate formula which, although related to standard charge-transfer theories, presents some original features and allows the determination of the rate at very low computational cost is developed. The curve-crossing results are compared to those of a path-integral, quantum transition-state calculation. The overall agreement between the two methods is satisfactory, although there is a discrepancy in the adiabatic reaction regime; a rigorous estimation of the transmission coefficients would be needed then. Finally, it is shown that zero-point energy and parabolic barrier tunneling factors added to the classical transition-state-theory rate constant are unable to describe properly the quantum effects in the present case.

I. INTRODUCTION

Proton-transfer equilibria in asymmetrical H-bonded complexes, and particularly those presenting an OH–N bond, have been studied extensively by various experimental means.[1,2] In the gas phase, these complexes are generally found in a neutral, covalent configuration, $AH-B$. In the presence of an external polar medium however, the ionic configuration $A^- - H^+ B$ may be stabilized by the electrostatic interactions, and a chemical equilibrium between covalent and ionic forms of the complex is then observable. This equilibrium is very sensitive to the electrostatic properties of the solvent and to the relative aciditic and basic characters of the compounds forming the complex. Theoretically, the main chemical features can be well fitted to a two-state valence-bond model.[3,4] The valence-bond perspective has led to a powerful empirical method (the so-called EVB method) for defining microscopic reaction potentials.[5,6] The EVB approach has been applied recently to the study of OH–N systems, either at a microscopic simulation level[7] or at a dielectric continuum level, with a self-consistent treatment of the solvent electronic polarization.[8]

When a tautomeric equilibrium $AH-B \rightleftharpoons A^- - H^+ B$ exists in solution, the problem of the associated proton-transfer rate constant arises. Rate constants for such equilibria have indeed been measured for phenol-amine complexes in various polar, aprotic solvents at low temperature. For these systems, the reaction is sufficiently slow to be traced by nuclear magnetic resonance (NMR).[9,10]

In this paper, we present a molecular dynamics (MD) study of a model for a proton-transfer reaction in a hydrogen-bonded $AH-B$ complex dissolved in liquid chloromethane (which has properties close to those of chloroethane, a typical solvent used in many experiments[10]).

There exists by now a number of theoretical approaches permitting one to cope with the quantum character of the proton at a simulation level. Those include diabatic curve-crossing approaches,[11,12] adiabatic quantum simulation techniques[13–18] and possible nonadiabatic extensions,[19,20] dispersed polaron models,[7] path-integral formulations,[7,21–26] and semiclassical tunneling algorithms.[27,28] Computational studies using these methods have helped us a great deal to understand many features of proton-transfer reactions in solution[7,12,14,15,18,21,26] and in biological systems.[21]

In this work, we pursue the same kind of study for proton transfer in $AH-B$ complexes. This type of proton transfer is to be distinguished from those occurring in ion–molecule complexes $AH^+ - B$, in intramolecular bonds (such as in the malonaldehyde molecule), or in symmetrical intermolecular complexes (such as acid dimers), by the fact that there is an extensive molecular rearrangement and charge reorganization accompanying the transfer.[29] The solvent effects are therefore expected to be much more important than in the other cases. For those complexes in fact, the reaction does not even exist without the presence of the solvent! In this context, the purpose of the present MD study is to provide a molecular picture of the static and dynamical role of the solvent in these reactions and to evaluate in the most rigorous way the tunneling contribu-

a)Author to whom correspondence should be addressed.

 0021-9606/93/097361-14$06.00

tion to the rate constant and the associated kinetic isotope effect (KIE).

The paper is organized as follows. In Sec. II, we present a molecular model describing an OH–N complex. The characteristics of the model have some flexibility, in order to reproduce the properties of complexes having different H-bond strengths and O–N equilibrium distances. The interaction with the molecular solvent is then introduced, and the solvation properties of the complex are discussed in terms of the "classical" free energy surface, computed by MD. In Sec. III, we derive a version of a semiclassical curve-crossing formula[30] suitable for MD simulation. The simulation formulation is based on the computation of a few standard charge-transfer quantities and presents several original features with respect to the strategy generally adopted in the literature. We then use the curve-crossing formula to compute the rate constant. We are able to outline the solvent contributions, characterize the adiabaticity of the reaction, and discuss the isotopic substitution effects. In Sec. IV, the rate constant is computed by using an independent path-integral route, and the results are compared to those of the curve-crossing calculation. In Sec. V, the tunneling contribution to the rate is evaluated by comparison to classical TST answers, corrected or not by zero-point energy (ZPE) and tunneling factors. Concluding remarks are offered in Sec. VI.

II. MOLECULAR DYNAMICS MODEL

A. Complex

Our study is devoted to a linear model for an $AH-B$ complex. The chemical groups A and B (standing for example for a ΦO and a NR_3 group) are modeled by two Lennard-Jones centers. The complex can be found in a covalent form or in an ionic form, noted A and B hereafter. In the covalent form, the proton is attached to A and the complex possesses a small dipole, associated mainly to the polarity of the A–H bond ($\mu_A=2.5$ D). In the ionic form, the proton becomes attached to B; the charge separation associated to the proton transfer results in a large value of the dipole moment ($\mu_B=10.5$ D).

The linear complex $AH-B$ is characterized by the position of the center of mass $\mathbf{R}_C$, the orientation unit vector $\mathbf{\Omega}$, and by the two internal distances $r=d_{AH}$, $R=d_{AB}$. The gas-phase Hamiltonian is written as

$$H_g=\tfrac{1}{2}I(R)\dot{\mathbf{\Omega}}^2+\tfrac{1}{2}M_c\dot{\mathbf{R}}_c^2+\tfrac{1}{2}M\dot{R}^2+\tfrac{1}{2}m\dot{r}^2+V_{HB}(r,R). \tag{1}$$

This Hamiltonian neglects the kinetic coupling between H and the overall translation rotation of the complex (an approximation justified by the condition $m\ll m_A,m_B$). $V_{HB}(r,R)$ is a potential energy surface describing the H-bonding interaction within the complex. It is taken in a pairwise additive form:

TABLE I. Parameters for the 3 model complexes described in Sec. II.

System	R_0	ΔH_0 (kcal/mole)	a (Å^{-1})	b (10^{13} kcal/mole)
(I)	2.75	6.0	10.7	2.40
(II)	2.7	7.8	11.2	7.1
(III)	2.65	10.0	11.8	21.0

$$V_{HB}(r,R)=be^{-aR}+D_A\left[1-\exp\left(\frac{-n_A(r-d_A)^2}{2r}\right)\right]+cD_A\left[1-\exp\left(\frac{-n_B(R-r-d_B)^2}{2(R-r)}\right)\right]. \tag{2}$$

This functional form was introduced by Lippincott and Schroeder in order to model the H-bond interaction between chemical groups of various kind.[31] The first exponential term accounts for the core repulsion between A and B. The second and third terms describe the chemical bonding of H with either A and B, and the resulting H-bonding attractive interaction between A and B. In this work, we have chosen the different parameters of the potential in order to reproduce the properties of phenol-amine complexes. $d_{A,B}$ and $n_{A,B}$ are fixed by the equilibrium bond distance and vibrational frequency of typical OH and N^+H bonds *in vacuo* ($d_A=d_{OH}=0.95$ Å, $d_B=d_{NH}=0.97$ Å, $\omega_A=\omega_{OH}=3650$ cm^{-1}, $\omega_B=\omega_{NH}=3550$ cm^{-1}). D_A is taken equal to the dissociation energy of OH bonds *in vacuo* ($D_A=D_{OH}=110$ kcal/mole) and the parameter c is adjusted to allow for a stabilization of the ionic complex in CH_3Cl, in agreement with the experimental situation for phenol-amine complexes in similar solvents. In order to explore different types of complex and to understand the influence of the strength of the AH–B bond on the proton-transfer characteristics, we have considered 3 different sets of parameters a,b, thus defining 3 different systems with increasing bond strength, noted hereafter (I)–(III). For the 3 systems, the parameters a,b have been selected to yield an equilibrium A-B distance, R_0, and an enthalpy of association, ΔH_0, in agreement with the experimental values for phenol-amine complexes ($R_0\approx 2.7$ Å, $\Delta H_0\approx 5-12$ kcal/mole). We have $R_0=2.75$ Å, $\Delta H_0=6$ kcal/mole for system (I), $R_0=2.7$ Å, $\Delta H_0\simeq 8$ kcal/mole for system (II), and $R_0=2.6$ Å, $\Delta H_0=10$ kcal/mole for system (III) (see the corresponding a,b parameters in Table I). The first system represents a rather weak OH–N bond, whereas the third one represents a rather strong bond.[32]

The potential $V_{HB}(r,R)$ is represented in Fig. 1(a) for system (II). Figure 1(b) presents a section of the surface at the equilibrium distance $R_0=2.7$ Å. At this distance, the potential exhibits a second minimum, locating the metastable ionic state. This minimum disappears at shorter distances. Figure 2 represents the potential in the covalent state as a function of R; the dissociation energy is around 8 kcal/mole in this case.

Another important ingredient of our model is the variation of the charge distribution, describing the transition from a covalent electronic state to an ionic one when the

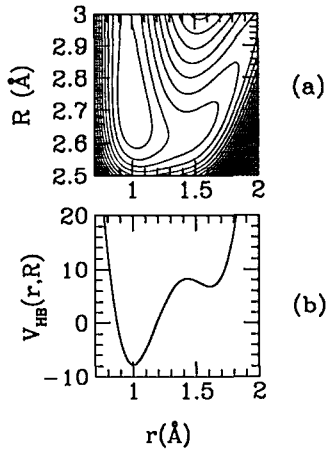

FIG. 1. Gas-phase H-bonding potential used in this work (model II). (a) Two dimensional plot; (b) section at $R=2.7$ Å.

proton is displaced from A to B. The charge variation is obtained by assigning a set of coordinate-dependent point charges on the sites A,H,B, in the form,

$$e_\alpha(r)=(1-f(r))e_\alpha^c+f(r)e_\alpha^i, \quad \alpha=A,H,B,$$

$$f(r)=\frac{1}{2}\left[1+\frac{r-r_0}{\sqrt{(r-r_0)^2+l^2}}\right], \tag{3}$$

with $r_0=1.43$ Å, the maximum of the gas-phase potential at $R=2.7$ Å, and $l=0.125$ Å.[33] The reactant, covalent state is defined by $e_A^c=-0.5e$, $e_H^c=+0.5e$, $e_B^c=0$ ($\mu_A=2.5$ D), whereas the product, ionic one is defined by $e_A^i=-e$, $e_H^i=+0.5e$, $e_B^i=+0.5e$ ($\mu_B=10.5$ D). From a charge-transfer perspective, the proton transfer can be viewed roughly as a neutral pair–ionic pair charge transition.

B. Complex and solvent

The complex described in the previous section is now considered as dissolved in liquid chloromethane. The solvent is modeled by an assembly of 255 polar, nonpolarizable molecules. The total Hamiltonian of the system may be decomposed as

$$H=H_g+T_S+V_{SS}+V_{LJ}(R,S)+V_c(r,R,S). \tag{4}$$

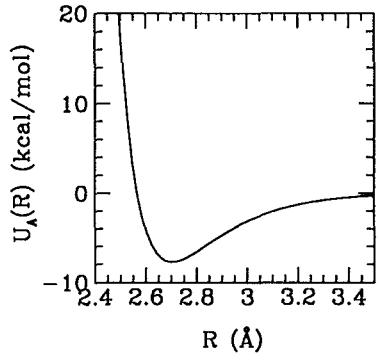

FIG. 2. Binding potential along the R coordinate in the covalent state.

We include in the notation S the translational and rotational coordinates of the solvent and the complex; T_S is the corresponding kinetic energy. V_{SS} represents the solvent–solvent interaction, in the form of site–site Lennard-Jones and Coulomb potentials. The methyl group of CH_3Cl is reduced to a single atomic site; the corresponding solvent parameters have been taken from the Monte Carlo simulations of Bigot *et al.*[34] The interaction of the solvent molecules with the complex is composed of a Lennard-Jones interaction V_{LJ} with the groups A and B ($\sigma_A=\sigma_B=3.5$ Å, $\epsilon_A=\epsilon_B=200$ K), and a Coulombic interaction V_c with the r-dependent charges on A, H, and B. We note that the interaction potential in Eq. (4) does not include either the electronic polarization of the solvent or that of the complex. For the latter, a substantial part of the polarizability comes from the valence-bond character of the OH–N interaction and could be incorporated in a simple way by using an EVB Hamiltonian. See Refs. 5, 8, and 35 and also Refs. 36 and 37 for related charge-transfer reactions. We think however that the Hamiltonian (4) contains a picture of the interactions involved that is sufficient for the purpose of the present study, namely, a description of the solvent influence on the rate and of the effect of the quantization of the proton. As a drawback, the model might underestimate the solute–solvent coupling. We reserve electronic polarization effects to a future work.

All the simulations described below were performed at $T=249$ K, $\rho=0.012$ Å^{-3}, close to the boiling point of chloromethane, in order to use a thermodynamical point already explored for the pure solvent.[34] The equations of motion were integrated using a leap-frog algorithm for the translations and a quaternion algorithm for the rotations. The masses of the groups A and B were taken as those of phenol ($m_A=93$) and trimethylamine ($m_B=59$). We have introduced a smooth truncation of the Coulombic interactions at $R_c=13.8$ Å, instead of using Ewald summations and dealing with all the nonphysical, periodic replicas of the complex.

C. Classical free energy surface

We have determined by MD the "classical free energy" of the complex, obtained by assimilating the proton to a classical entity. This quantity is defined by

$$W(r,R)=V_{HB}(r,R)+W_S(r,R)+2k_BT\ln(R/R_0). \tag{5}$$

The last term is the contribution of the rotational, centrifugal force, supposed independent of the proton coordinate. The second term represents the solvation free energy, which can be computed in simulation by integrating the mean force exerted on the internal coordinates:

$$W_S(r,R')=W_S(r_0,R')-\int_{r_0}^{r}dr'\langle F_r(r',R')\rangle_c, \tag{6}$$

$$W_S(r',R)=W_S(r',R_0)-\int_{R_0}^{R}dR'\langle F_R(r',R')\rangle_c, \tag{7}$$

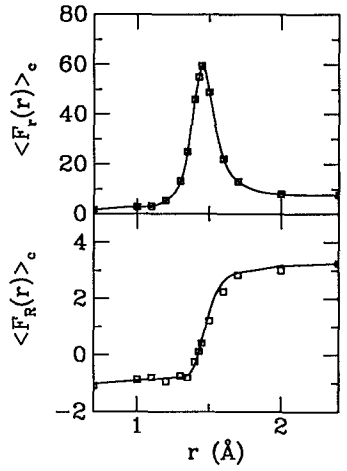

FIG. 3. Mean external forces along the internal coordinates at $R=2.7$ Å. The squares are the simulation results. The solid lines represent analytical polynomial fits.

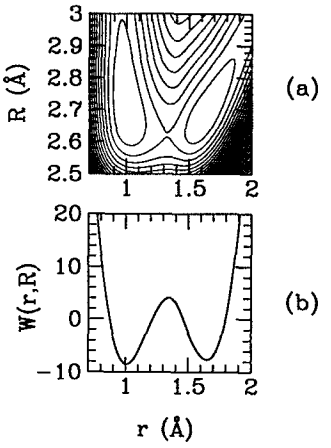

FIG. 4. Same as Fig. 1 for the classical free energy of the solvated complex (model II).

where $\langle F_x(r',R')\rangle_c$ indicates an average of the Lennard-Jones and Coulombic forces on $x=r,R$ performed with the constraints $r=r'$ and $R=R'$. Since the mass of H is negligible with respect to those of A and B, these forces are related to the forces on the atomic sites by

$$F_r=\mathbf{F}_H.\mathbf{\Omega}-\sum_{\alpha=A,H,B}\frac{de_\alpha}{dr}V_\alpha, \tag{8}$$

$$F_R=\left(\frac{m_A}{m_A+m_B}\mathbf{F}_B-\frac{m_B}{m_A+m_B}(\mathbf{F}_A+\mathbf{F}_H)\right).\mathbf{\Omega}, \tag{9}$$

where $\mathbf{\Omega}$ is the orientation unitary vector, pointing from A to B, and V_α represents the value of Coulombic potential at site α. The mean forces were determined at a few selected values of R by performing 15 runs with the proton position r varying from 0.7 to 2.6 Å. Each run consisted of an equilibration period of 3 ps and an integration period of 40 ps, with a time step of 0.01 ps. We have found that in the region of R which is important for describing the proton-transfer reaction (2.5 Å $<R<$ 3.0 Å) the solvation free energy is very well approximated by the expansion

$$W_S(r,R)=W_S(r_0,R_0)-\int_{r_0}^{r}dr'\langle F_r(r',R_0)\rangle_c$$
$$-\langle F_R(r,R_0)\rangle_c(R-R_0), \tag{10}$$

with $R_0=2.7$ Å. The mean forces are plotted in Fig. 3. The force along the proton coordinate r presents a sharp maximum at r_0, the location of the inflexion point of the charge switching function defined in Eq. (3). The force along R varies rapidly in the same region, marking the transition between weak and strong Coulombic interaction with the polar solvent.

A contour plot of the resulting total free energy surface $W(r,R)$ is given in Fig. 4(a) for system (II); a section at $R_0=2.7$ Å is presented in Fig. 4(b). Compare to the corresponding figures in the gas phase (Fig. 1). It can be seen that, for the model considered, the interaction with the solvent is able to stabilize the ionic species and create a tautomeric equilibrium between the covalent and ionic forms of the complex. The situation is then comparable to the experimental observations for phenol-amine complexes described in the Introduction.[9,10]

At $R=2.7$ Å, the stabilization by the solvent has diminished the energy gap between covalent and ionic states to about 1 kcal/mole, there is a 12 kcal/mole barrier separating the two wells. The barrier decreases very rapidly with R: It is only 6 kcal/mole at $R=2.6$ Å and disappears completely for $R<2.5$ Å. The strong R dependence of the barrier height is characteristic of H-bonded systems and, as emphasized already in a number of theoretical works,[11,38–40] this feature has some important implications on the proton-transfer mechanism.

For system (II), the saddle point of the two-dimensional surface turns out to be at the same level than the dissociation energy of the complex. The saddle point is located above the dissociation threshold for system (I) and under it for system (III). The three systems span therefore the different possible experimental situations.

We conclude this section by a remark concerning the physical content of the "classical free energy" surface $W(r,R)$: the proton is indeed a quantum entity and, as will be discussed hereafter, this quantum character has important consequences on the properties of the system. However, as we have seen, $W(r,R)$ offers a convenient way to discuss the stabilization of the ionic complex. On the other hand, this surface is useful to compare rigorous quantum calculations to a classical reference, corrected or not by zero-point-energy and tunneling factors. We will come back to this point later.

III. CURVE-CROSSING APPROACH

A. Rate formula

Following earlier works on electronic charge-transfer systems[35,41–44] as well as proton-transfer reactions in solution,[11,14,15] we adopt in this section a semiclassical point of view. Since the proton motion is much faster than that of the other degrees of freedom, including the distance R and all the solvent coordinates, a Born–Oppenheimer approxi-

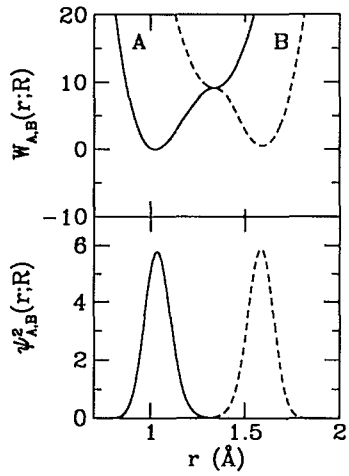

FIG. 5. Diabatic potentials defined in Eqs. (11) and (12) and associated diabatic ground-state probability densities ($R=2.65$ Å).

mation scheme can be used. The Schrödinger equation for the proton is first solved at fixed $(R,\mathbf{S})$ coordinates, and parametric wave functions $\Psi_n(r;R,\mathbf{S})$ are obtained. The quantum system is then represented by a set of "protonically adiabatic" Hamiltonians $H_n=\langle\Psi_n|H|\Psi_n\rangle$, describing the classical motion of the slow coordinates $(R,\mathbf{S})$ when the proton is in its nth excited state. Corrections to the Born–Oppenheimer approximation can be accounted for by introducing a semiclassical hopping process between the adiabatic potential energy surfaces. Rather elaborated semiclassical algorithms are available in the literature,[19,20] which may be applied to our problem.

In order to determine the multidimensional adiabatic surfaces for the classical coordinates, we adopt here a variational strategy, rather than the straight solution developed in one of our previous works.[14] We define the variational, adiabatic states in the following way. For each value of the separation distance R, we consider two solvent-independent diabatic potentials, defined from the classical free energy surface $W(r,R)$ by

$$W_A(r,R)=W(r,R);$$

$$W_B(r,R)=W(r_b(R),R)+W_c(r,R), \quad r<r_b(R), \tag{11}$$

$$W_A(r,R)=W(r_b(R),R)+W_c(r,R);$$

$$W_B(r,R)=W(r,R), \quad r>r_b(R), \tag{12}$$

where $r_b(R)$ denotes the position of the barrier top at given R. W_c is an arbitrary confining potential, which verifies $W_c(r_b(R),R)=0$, and allows for a definition of the diabatic potentials beyond the barrier top (see Fig. 5).

The eigenstates of the diabatic potentials are then used to define two complete sets of variational, diabatic wave functions, $\Psi^{(n)}_{A,B}(r;R)$. Those two diabatic sets make it possible to account for diabatic transitions from or to excited protonic vibrational levels (or, in an adiabatic perspective, for the motion on adiabatic surfaces higher than the ground and first-excited ones). We could verify however that, for our model, the excited states play a negligible role in the computed proton-transfer rate constant; the contribution is still small, although not completely negligible for deuterium. For sake of simplicity, the discussion will therefore be restricted to the two ground diabatic states, $\Psi_{A,B}(r;R)\equiv\Psi^{(0)}_{A,B}(r;R)$, and to the associated ground and first-excited adiabatic states.

When expressed in the diabatic basis set, the total Hamiltonian of Eq. (4) is represented by the following 2×2 matrix[44,45]

$$H=\begin{pmatrix} H_A & C \\ C & H_B \end{pmatrix}, \tag{13}$$

where

$$H_{A,B}=T_S+T_R+E_{A,B}(R,\mathbf{S}), \tag{14}$$

$$C(R,\mathbf{S})=\frac{2H_{AB}-S_{AB}(E_A+E_B)}{2(1-S^2_{AB})}, \tag{15}$$

with the definitions,

$$E_{A,B}(R,\mathbf{S})=\langle\Psi_{A,B}|H|\Psi_{A,B}\rangle,$$

$$S_{AB}(R,\mathbf{S})=\langle\Psi_A|\Psi_B\rangle, \tag{16}$$

$$H_{AB}(R,\mathbf{S})=\langle\Psi_A|H|\Psi_B\rangle.$$

In the latter expressions, H is taken at fixed $(R,\mathbf{S})$ coordinates. The adiabatic Hamiltonians corresponding to Eqs. (13)–(16) read

$$H_{0,1}=\tfrac{1}{2}[H_A+H_B\pm\sqrt{\Delta E^2(R,\mathbf{S})+4C^2(R,\mathbf{S})}], \tag{17}$$

with $\Delta E=E_A-E_B$. As pointed out in many studies on charge transfers in polar media,[12,35,41–44,46] $\Delta E(R,\mathbf{S})$ appears as a natural and convenient collective coordinate for characterizing the solvent influence on the reaction process. In the two-state perspective developed above, the quantum-mechanical forward rate constant may be written, following Borgis and Hynes,[30] by choosing the Landau–Zener transition-state value as a reference TST value:

$$k_{LZ}=\kappa_{LZ}\cdot k^{TST}_{LZ}$$

$$=\kappa_{LZ}\cdot\frac{Q_0}{Q_A}\langle\Delta\dot{E}\Theta(\Delta\dot{E})\delta(\Delta E)P_{LZ}(\Delta\dot{E})\rangle_0. \tag{18}$$

k^{TST}_{LZ} is the rate expression obtained by (i) representing the quantum hopping process by a Landau–Zener process, in which a probability of transition from one adiabatic surface to the other can be assigned at each crossing event, and (ii) neglecting the dynamical influence of the coordinates coupled to ΔE. In Eq. (18), $\langle\cdot\rangle_0$ indicates an adiabatic ground-state average. Q_0 is the adiabatic ground-state partition function and Q_A is the equivalent quantity in the reactant region, defined by $\Delta E<0$. $\Theta(\Delta\dot{E})$ denotes the Heaviside function and selects the forward trajectories, going from A to B. Finally, $P_{LZ}(\Delta\dot{E})$ is the Landau–Zener probability that a trajectory coming from the ground-state reactant region, and reaching the transition state $\Delta E=0$ with velocity $\Delta\dot{E}$, ends in the ground-state product region after the crossing:[45,47]

$$P_{LZ}(\Delta\dot{E})=\frac{1-\exp(-\gamma_{LZ}(\Delta\dot{E}))}{1-\frac{1}{2}\exp(-\gamma_{LZ}(\Delta\dot{E}))}, \quad \gamma_{LZ}(\Delta\dot{E})=\frac{2\pi C^2}{\hbar\Delta\dot{E}}. \tag{19}$$

In the nonadiabatic limit in which, for any $(R,\mathbf{S})$ configuration contributing to the reaction, the Landau–Zener parameter γ_{LZ} is small ($\gamma_{LZ}<1$), the transition-state rate constant reads

$$k_{LZ}^{TST}=\frac{Q_0}{Q_A}\frac{4\pi}{\hbar}\langle C^2\Theta(\Delta\dot{E})\delta(\Delta E)\rangle_0=\frac{2\pi}{\hbar}\langle C^2\delta(\Delta E)\rangle_A. \tag{20}$$

Apart some subtleties regarding the definition of the reactant partition function, the latter formula is identical to that which can be obtained from a rigorous time-dependent formula, including all dynamical effects, with the only assumption that R and $\mathbf{S}$ are classical variables. In this case, the transmission coefficient κ_{LZ} in Eq. (18) is equal to 1. See, e.g., Ref. 11 and Appendix A of Ref. 23. In the opposite, adiabatic limit ($\gamma_{LZ}>1$), the dynamics is confined to the ground-state potential surface and the corresponding adiabatic transmission coefficient κ_{LZ}^0 can be computed exactly by MD. In the light of previous studies for related systems,[14,15,44] it can be anticipated that κ_{LZ}^0 is a quantity not very different from 1.

We will thus focus in the following on the transition-state value k_{LZ}^{TST}. This latter can be conveniently rewritten as

$$k_{LZ}^{TST}=\frac{Q_0}{Q_A}\int dR'\, g_0(R')\langle\delta(\Delta E)\rangle_{0,\{R'\}} \times\langle\Delta\dot{E}\Theta(\Delta\dot{E})P_{LZ}(\Delta\dot{E})\rangle_{0,\{R',\Delta E=0\}}, \tag{21}$$

where $g_0(R')=\langle\delta(R-R')\rangle_0$ is the adiabatic ground-state probability distribution function for R. $\langle\delta(\Delta E)\rangle_{0,\{R'\}}=\langle\delta(\Delta E)\delta(\mathrm{R}-\mathrm{R}')\rangle_0/\langle\delta(\mathrm{R}-\mathrm{R}')\rangle_0$ is an activation term defined conditionally at $R=R'$, and the average over $\Delta\dot{E}$ is a reactive flux term, to be determined conditionally at $R=R'$ and $\Delta E=0$. All those terms can be computed exactly by using, e.g., constraint dynamics[48,49] or umbrella sampling.[50]

Instead of this direct but time-demanding computation, we follow an easier route, which relies on the following approximate properties (i)–(ii) of the system that we consider.

(i) If we define the "intermediate Hamiltonian" $H_{\dot{I}}=\frac{1}{2}(H_A+H_B)$, then the time-dependent variables $\Delta E^{(\dot{I})}(t)$, $\Delta\dot{E}^{(\dot{I})}(t)$, where $(\dot{I})$ indicates a dynamics associated to $H_{\dot{I}}$, realize two independent Gaussian processes at any fixed value of R. In particular, an effective Hamiltonian for the intermediate system $(\dot{I})$ may be defined in the following form:

$$\begin{aligned}H_{\dot{I}}(\Delta E,\Delta\dot{E},R')&=-k_BT\ln[\langle\delta(\Delta E(R,S)-\Delta E)\\&\quad\times\delta(\Delta\dot{E}(R,\dot{R},\mathbf{S},\dot{\mathbf{S}})-\Delta\dot{E})\delta(R-R')\rangle_{\dot{I}}]\\&=G_{\dot{I}}(R')+\frac{1}{2}\frac{k_BT}{\langle\Delta\dot{E}^2\rangle_{\dot{I},\{R\}}}\Delta\dot{E}^2\\&\quad+\frac{1}{2}\frac{k_BT}{\langle\delta\Delta E^2\rangle_{\dot{I},\{R\}}}(\Delta E-\langle\Delta E\rangle_{\dot{I},\{R\}})^2,\end{aligned} \tag{22}$$

where $\langle\cdot\rangle_{\dot{I},\{R\}}$ denotes an average taken with $H_{\dot{I}}$ at fixed R and $G_{\dot{I}}(R)$ is an R-dependent free energy term. The Gaussian character of ΔE has been emphasized for a number of charge-transfer studies in solution, but is usually considered as a property of the diabatic states. We note that, as stated here, i.e., referring to the intermediate Hamiltonian rather than H_A or H_B, the Gaussian property of ΔE yields the exact relationship,[42,51]

$$G_A(\Delta E,R)=G_B(\Delta E,R)+\Delta E, \tag{23}$$

where $G_{A,B}$ are the diabatic solvent free energies (see Appendix A for a proper definition and derivation). This is not the case when H_A or H_B are used as reference states instead of $H_{\dot{I}}$, at least for nonsymmetrical charge-transfer systems.[51] Furthermore, a Marcus relationship between nonadiabatic activation free energy and reaction free energy can be recovered in the form,

$$\Delta G^{\ddagger}(R)=\frac{(\Delta G(R)+E_r(R))^2}{4E_r(R)}, \tag{24}$$

where, for each value of R, the reaction free energy $\Delta G(R)$ and the solvent reorganization energy $E_r(R)$ are defined in microscopic terms by

$$\Delta G(R)=-\langle\Delta E\rangle_{\dot{I},\{R\}}=-\tfrac{1}{2}(\langle\Delta E\rangle_{A,\{R\}}+\langle\Delta E\rangle_{B,\{R\}}), \tag{25}$$

$$E_r(R)=\frac{1}{2}\frac{\langle\delta\Delta E^2\rangle_{\dot{I},\{R\}}}{k_BT}=\frac{1}{2}(\langle\Delta E\rangle_{B,\{R\}}-\langle\Delta E\rangle_{A,\{R\}}). \tag{26}$$

In these equations, the last term involves an average over the diabatic states A and B (see Appendix A). The microscopic validity of the Marcus relationship has been tested numerically for various asymmetrical charge-transfer systems in aprotic and protic solvents.[42] This gives support to the Gaussian approximation developed above.

(ii) The second property to be used is the possible decomposition of the diabatic coupling $C(R,\mathbf{S})$ as

$$C(R,\mathbf{S})=C_0(R)+C_1(R)\Delta E(R,\mathbf{S}), \tag{27}$$

where $C_0(R)$ is an effective solvent-independent coupling, defined at $\Delta E=0$. This expression of the coupling is justified in Appendix B; it is exact at dominant order in the electrostatic complex-solvent coupling.

By using the two properties just described, Eqs. (22),(27), and also Eqs. (17),(24),(25),(26), the activation term in Eq. (21) becomes

$$\langle\delta(\Delta E)\rangle_{0,\{R\}}=\frac{\langle\exp((\beta/2)\sqrt{\Delta E^2+4C^2})\delta(\Delta E)\rangle_{i,\{R\}}}{\langle\exp((\beta/2)\sqrt{\Delta E^2+4C^2})\rangle_{i,\{R\}}}$$

$$=\frac{\exp(-\beta\Delta G^2(R)/4E_r(R)+\beta C_0(R))}{\int d\Delta E\exp(-[\beta(\Delta E+\Delta G(R))^2]/4E_r(R)+(\beta/2)[\Delta E^2+4(C_0(R)+C_1(R)\Delta E)^2]^{1/2})}. \quad (28)$$

Taking into account the fact that $C\ll|\Delta E|$ in the regions contributing to the partition function in the denominator, we recover a familiar, "Marcus-like" expression,

$$\langle\delta(\Delta E)\rangle_{0,\{R\}}=\left(\frac{\beta}{4\pi E_r(R)}\right)^{1/2}\frac{e^{-\beta[\Delta G^{\ddagger}(R)-C_0(R)]}}{1+e^{-\beta\Delta G(R)}}, \quad (29)$$

in which the activation term involves the nonadiabatic, reactant activation energy $\Delta G^{\ddagger}(R)$ of Eq. (24), corrected by the diabatic coupling $C_0(R)$.[52]

The conditional reactive flux term in Eq. (21) can also be computed easily from the effective Hamiltonian H_i of Eq. (22). It can be put in the form,[30]

$$\langle\Delta\dot{E}\Theta(\Delta\dot{E})P_{LZ}(\Delta\dot{E})\rangle_{0,\{R,\Delta E=0\}}$$

$$=\left(\frac{\omega_S^2(R)E_r(R)}{\pi\beta}\right)^{1/2}\bar{P}_{LZ}(R), \quad (30)$$

where $\bar{P}_{LZ}$ is an effective Landau–Zener crossing probability at a given R:

$$\bar{P}_{LZ}(R)=\frac{\beta}{2\omega_S^2(R)E_r(R)}\int_0^{+\infty}d\Delta\,\dot{E}\Delta\dot{E}P_{LZ}(\Delta\dot{E})$$

$$\times\exp\left(-\frac{\beta\Delta\dot{E}^2}{4\omega_S^2(R)E_r(R)}\right). \quad (31)$$

In these expressions, we have introduced the R-dependent solvent frequency

$$\omega_S(R)=\sqrt{\frac{\langle\Delta\dot{E}^2\rangle_{i,\{R\}}}{\langle\delta\Delta E^2\rangle_{i,\{R\}}}}. \quad (32)$$

Gathering Eqs. (18) and (29)–(32), we find the following final expression for k_{LZ}^{TST}

$$k_{LZ}^{TST}=\int_0^{+\infty}dR\,g_A(R)k_{LZ}^{TST}(R), \quad (33)$$

$$k_{LZ}^{TST}(R)=\frac{\omega_S(R)}{2\pi}\cdot\bar{P}_{LZ}(R)\cdot e^{-\beta[\Delta G^{\ddagger}(R)-C_0(R)]}. \quad (34)$$

Similar formulas are derived in Ref. 30. In Eq. (33),

$$g_A(R')=\frac{Q_0}{Q_A}\frac{\langle\delta(R-R')\rangle_0}{1+e^{-\beta\Delta G(R)}}$$

$$=\frac{\langle\delta(R-R')(1-\Theta(\Delta E))\rangle_0}{\langle1-\Theta(\Delta E)\rangle_0} \quad (35)$$

is the probability distribution function for R in the reactant region, $\Delta E<0$. Rate formulas similar to Eqs. (33) and (34) are familiar in the context of electron-transfer reactions,[45] and have been applied to the treatment of proton-transfer reactions in solution by German *et al.*[53] (For a review, see also Ref. 54.) However, there are a few basic differences between the rate formula proposed by the latter authors and Eq. (34). First, our approach is based on an adiabatic, avoided crossing perspective ($i-e$, a Landau rather than a Zener perspective), which brings a coupling correction to the solvent activation energy in the adiabatic limit. Second, the effective Landau–Zener crossing probability $\bar{P}_{LZ}$ results in our case from an average over individual, microscopic trajectories, and it differs slightly from the definition taken by German *et al.*[53] Finally, the important parameters of the problem, the solvent reorganization energy, the reaction free energy, and the quantum-mechanical coupling are defined here for a microscopic model rather than a phenomenological one, and we provide a proper, easy way to compute all these quantities at a true, microscopic level, using for instance MD simulations.

B. Computational details

In order to define the diabatic potentials of Eqs. (11) and (12), we have chosen an harmonic confining potential,

$$W_c(r,R)=\tfrac{1}{2}m\omega_b(R)(r-r_b(R))^2, \quad (36)$$

where $\omega_b(R)$ is the barrier frequency of $W(r,R)$. The corresponding diabatic states are depicted in Fig. 5. The choice of W_c is somehow arbitrary. Nevertheless, when the diabatic energy levels are below the barrier top of $W(r,R)$, even close to it, the diabatic states defined this way are indeed very close to the WKB, semiclassical ones, and they are independent of W_c. At short R separation, when the barrier of $W(r,R)$ is small and the diabatic states do not exist in a WKB sense, the definition of $\Psi_{A,B}$ from the diabatic potentials $W_{A,B}$ is still possible and provides a convenient, variational basis set. The resulting diabatic picture is then weakly dependent on W_c.

The diabatic states being defined, it is possible to compute the solvent-independent coupling $C_0(R)$ of Eq. (27). The resulting function is plotted in Fig. 6. We find that at large R separation ($R>2.8$ Å), $C_0(R)$ is well represented by an exponential function

$$C_0(R)=C_0\exp(-\alpha(R-R_0)), \quad (37)$$

with $\alpha\simeq39$ Å^{-1}.[55] This simple exponential form of the coupling at large distances is a general feature of H-bonded systems. It has been used as a phenomenological input in the theoretical description of proton-transfer reactions in molecules and complexes involving a large separation between donor and acceptor atoms.[11,12,38] At short distances ($R<2.8$ Å), the behavior of $C_0(R)$ is no longer exponential, and can be described by a polynomial law.[30] We note

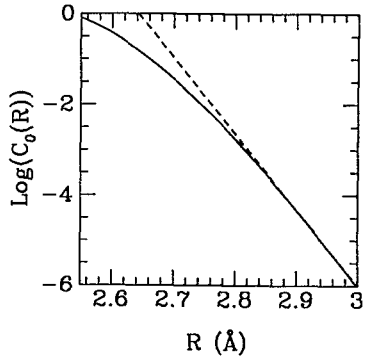

FIG. 6. Solvent-dependent diabatic coupling as a function of R. The dashed straight line represents the exponential limit of Eq. (37), which is valid for large values of R.

that the 3 complexes studied in this work are characterized by relatively short equilibrium distances ($R_0 \leqslant 2.75$ Å), so that the exponential form of the coupling is not applicable.

The projection of the total Hamiltonian onto the diabatic states $\Psi_{A,B}(r;R)$ leads to the definition of two different dynamical processes, associated to the diabatic Hamiltonians $H_{A,B}$ of Eq. (14) (and to the definition of the intermediate process, associated to $H_{\bar{I}}$). These dynamical processes are purely classical ones: once the quantum character of the proton has been dealt with by defining the proper diabatic functions $\Psi_{A,B}(r;R)$, the interaction of the solvent with the solute charge distribution is reduced to a classical Coulombic interaction with two point charges $\langle e_\alpha \rangle_{A,B} = \langle \Psi_{A,B} | e_\alpha(r) | \Psi_{A,B} \rangle$ on the sites $\alpha = A,B$, complemented by a set of distributed point charges $e_{H,i} = e_H \Psi^2_{A,B}(r_i;R)dr$, placed at regular sites $r_i = i \cdot dr$ along the A-B axis, and representing the delocalized proton. In a diabatic simulation at fixed R, the complex is therefore assimilated to a *rigid* molecule carrying a *fixed* point-charge distribution. The MD simulation procedure is therefore straightforward.

Conformably to the previous lines, we have computed the solvent reorganization energy $E_r(R)$ and the reaction free energy $\Delta G(R)$ for different values of R. We have used the second equality of Eqs. (25) and (26) which requires the computation of the average of ΔE in the diabatic states and avoids the need of any fluctuation term. Two simulations, one with H_A and one with H_B, were carried out for a series of values of R ranging from $R = 2.55$ Å to $R = 2.8$ Å, thus spanning the region important for the reaction. Accurate values of $E_r(R)$ and $\Delta G(R)$ were obtained from rather short runs (typically 25 ps). Similar runs with $H_{\bar{I}}$ were used to evaluate the R-dependent solvent frequency $\omega_S(R)$ from Eq. (32); the uncertainty is larger then, since the formula involves the ratio of two fluctuation terms. The different results are reported in Table II. We find, in particular, that the solvent reorganization energy is always proportional to the square of dipole difference, $\Delta\mu^2 = [\langle \Psi_B | \mu | \Psi_B \rangle - \langle \Psi_A | \mu | \Psi_A \rangle]^2$, which indicates the predominance of the dipolar interactions in our model. The values of the solvent frequency are a little bit scattered but

TABLE II. Charge-transfer quantities computed at different values of the A-B distance by the MD method described in Sec. III.

R (Å)	$\Delta\mu$ (D)	ΔG (kcal/mole)	E_r (kcal/mole)	$E_r/\Delta\mu^2$	ω_S (ps^{-1})
2.6	5.15	1.45	3.65	0.14	9.1
2.65	6.30	0.80	5.45	0.14	8.2
2.7	7.05	0.75	6.90	0.14	8.7
2.8	8.15	1.40	8.50	0.13	8.9

seem rather independent of R. We have adopted a mean value of $\omega_S(R) = \omega_S = 8.75$ ps^{-1} in our rate calculations.

C. Simulation results

The previous quantities being determined, the overall proton-transfer rate constant can be calculated from Eqs. (33) and (34). In order to understand the adiabatic/nonadiabatic character of the reaction, it is instructive to discriminate among the various R contributions, and to focus on the R-dependent Landau–Zener crossing probability $\bar{P}_{LZ}(R)$ of Eq. (31). The corresponding function, computed from the simulation results for $E_r(R)$ and $\omega_S(R)$, is presented in Fig. 7. A rather sharp transition occurs between $R = 2.7$ and $R = 2.6$ Å, marking the passage from a nonadiabatic limit of the reaction, in which $\bar{P}_{LZ}(R) \propto C_0^2(R)$, to an adiabatic one, in which $\bar{P}_{LZ}(R) = 1$. In the first region, the reaction is dominated by tunneling, whereas in the second one, the proton transfer is expected to be driven by the dynamics of the slow modes, including the solvent and the slow internal coordinate.[13,53,54]

The R-dependent rate of Eq. (34) is then plotted in Fig. 8. Since the reaction is facilitated by small potential barriers in the proton coordinate, $k_{LZ}^{TST}(R)$ increases drastically when going to short R separations. However, this general trend is much more pronounced in the nonadiabatic region. Two factors contribute there: first, the prefactor containing the square of the coupling increases almost exponentially (see Fig. 6). Second, the nonadiabatic

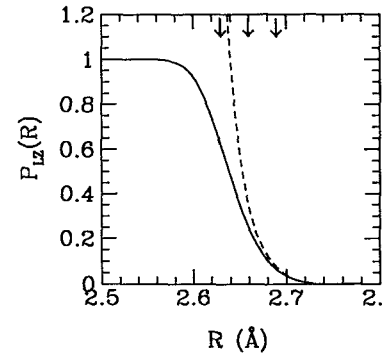

FIG. 7. Effective Landau–Zener crossing probability $\bar{P}_{LZ}(R)$ as a function of R [see Eqs. (30) and (31)]. The dashed line represents the nonadiabatic limit, $\bar{P}_{LZ}(R) = [2\pi/\hbar\omega_S(R)]\sqrt{[\beta/E_r(R)]}C_0^2(R)$. The arrows on top indicate the optimum reaction distances R^* for the three model complexes described in the text [(I)–(III) from right to left].

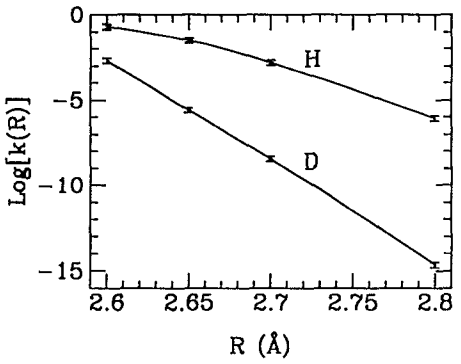

FIG. 8. Curve-crossing rate constant as a function of R for proton and deuterium. The simulation results and associated error bars are given for several values of R. The solid lines represent polynomial interpolations.

activation energy, which is governed mainly by the solvent reorganization energy, becomes less important when the complex is shrunk. In the adiabatic region, only the second effect remains; the prefactor is almost constant and proportional to the solvent frequency.

The results for the overall, integrated rate constant k_{LZ}^{TST} are given in Table III for the 3 model complexes (I)–(III) of Sec. II. Remember that (I) represents a model for a relatively weak H-bonded complex, with a long equilibrium distance between A and B, whereas (III) covers the opposite limit of a strong OH–N complex with a short A-B equilibrium distance. The rate values that we get go from the microsecond range for the weakest complex to the nanosecond range for the strongest one. Those rate constants are high compared to those found experimentally by Ratajczak *et al.*[10] However, their experiments are at much lower temperature and we need to include temperature effects in a future work.

We have also estimated the kinetic isotope effect (KIE) by applying the procedure described in the preceding sections to a complex in which the proton is replaced by a deuterium (see Fig. 8). The corresponding computed isotope effect is given in Table III for the 3 models; it varies from 150 for the complex with the weakest H bond to ~ 10 for the complex with the strongest one. KIE values larger than 20 are rarely observed for intermolecular complexes.[56,57] This remark indicates that, in the framework of the Lippincott–Schroeder potential adopted in this work, parameters close to those of our models (II) and (III) have some relevance for describing intermolecular OH–N complexes, whereas those of model (I) have been pushed towards the intramolecular case, in order to explore the situation of a fully nonadiabatic reaction, with important tunneling contributions (see below).

We note finally that the integrated rate constant k_{LZ}^{TST} can be understood as the result of two competing effects. The transfer of the proton is greatly facilitated at short A-B distance [$k_{LZ}^{TST}(R)$ increases with decreasing R's], but an exponential core repulsion between A and B is encountered then, which favors larger R distances. The repulsion effect is contained in the probability factor $g_A(R)$ of Eq. (21). The balance between the two effects is at the origin of a rather sharp maximum in the product $g_A(R)\cdot k_{LZ}^{TST}(R)$, occurring at some position R^*. The value of R^* may serve as a measure of the overall adiabatic character of the reaction, as indicated in Fig. 7 for the 3 model complexes (I)–(III). Model (I) is clearly in the nonadiabatic limit and model (III) is close to the adiabatic one; model (II) covers an intermediate situation. This classification should be put in parallel with the computed values of the KIE: small isotope effects are the manifestation of an adiabatic process, whereas large ones indicates a dominance of the nonadiabatic transitions. Many intermolecular proton transfers between oxygen and nitrogen atoms are likely to be in the adiabatic limit, with a small associated isotope effect.[56] In the present case, the sensitivity of the isotopic effect on R^* is probably too pronounced, a drawback of the Lippincott–Schroeder functional adopted in this work.[55] The basic trends are believed to be correct however.

IV. PATH-INTEGRAL CALCULATION

In order to confront the curve-crossing results to an independent calculation, we have computed the proton-transfer rate constant for our models by implementing a MD version of the centroid approach pioneered by Gillan,[22] and reformulated by Voth *et al.*[23–25] In a path-integral perspective,[58] the static, thermodynamical properties of the quantum system that we consider can be obtained from the discretized Hamiltonian

TABLE III. Simulation results for the 3 systems defined in Sec. II. The values of the rate constants are given in s^{-1}. R^* represents the optimum reaction distance (see the text and Fig. 7; compare also to the corresponding equilibrium distance R_0 in Table I). For each method, the value of the computed kinetic isotope effect is given in parentheses. The last column gives an estimation of the relative difference of effective activation energy found between the curve-crossing and path-integral integral calculations. This quantity is defined in reference to the adiabatic curve-crossing result, i.e., $\Delta W_{eff} = -k_B T \ln(2\pi/\omega_S \cdot k)$; tunneling contributions are thus incorporated in the activation energy itself.

System	R^*	k_c (ZPE)	k_c (ZPE+T)	k_{LZ}^{TST}	k_Q^{TST}	$\left\lvert\frac{\ln(k_{LZ}/\omega_S)-\ln(k_Q/\omega_S)}{\ln(k_{LZ}/\omega_S)}\right\rvert$
(I)	2.68	3.1×10^5 (7.7)	4.2×10^6 (43)	7.6×10^8 (150)	9.65×10^8 (130)	2.5%
(II)	2.65	8.6×10^6 (6.9)	7.7×10^7 (27)	7.8×10^9 (46)	10.5×10^9 (40)	4.0%
(III)	2.62	5.9×10^8 (5.6)	3.2×10^9 (15)	3.9×10^{10} (12)	8.2×10^{10} (13)	15.0%

$$H_Q=\sum_{i=1}^{N}\left[\frac{1}{2}\mu\dot{r}_i^2+\frac{1}{2}\frac{mN}{(\beta\hbar)^2}(r_{i+1}-r_i)^2+\frac{1}{N}[V_{HB}(r_i,R)+V_c(r_i,R,\mathbf{S})]\right]+T_R+T_S+V_{SS}+V_{LJ}(R,\mathbf{S}). \tag{38}$$

The notations correspond to those of Eq. (4). In this formulation, the variables R and $\mathbf{S}$ are treated classically. The proton is replaced by a necklace of N harmonically connected beads, $N\to\infty$. The kinetic terms associated to the r_i's, and the corresponding mass μ, are arbitrary and are introduced in order to allow for a MD sampling of phase space. Following Voth *et al.*,[23,24] we can formulate the quantum rate constant using the centroid of the proton thermal path,

$$\xi=\frac{1}{N}\sum_{i=1}^{N}r_i,$$

as the reaction coordinate:

$$k_Q=\kappa_Q\cdot k_Q^{\mathrm{TST}}, \tag{39}$$

$$k_Q^{\mathrm{TST}}=\frac{1}{2}\bar{v}\cdot\frac{Z}{Z_A}\langle\delta(\xi-\xi^{\ddagger}(R))\rangle. \tag{40}$$

In this expression, $\frac{1}{2}\bar{v}=(2\pi\beta m)^{-1/2}$ is the classical thermal velocity. $\xi^{\ddagger}(R)$ designates the maximum of the free energy along ξ at a given R. Z denotes the total partition function, and Z_A is the partition function of the reactant region, $Z_A=\langle(1-\Theta(\xi-\xi^{\ddagger}(R))\rangle$. κ_Q is a quantum transmission coefficient, which has a well defined expression in terms of a quantum time correlation function with complex weighting functional.[23] In this paper, we will consider only the quantum transition-state limit, $\kappa_Q=1$. This limit relies entirely upon the determination of the free energy surface for the variables ξ and R, $\bar{W}(\xi,R)$. A related path-integral study of proton and hydride transfers was performed by Warshel *et al.*, who used the energy gap along the centroid path as a reaction coordinate, instead of the centroid itself.[7,21]

We have computed the surfaces $\bar{W}(\xi,R)$ for our models by using MD simulations based on the Hamiltonian H_Q of Eq. (38). The quantum proton was modeled by a necklace of $N=30$ beads of mass $\mu=5$ amu. The whole free energy surface was constructed by integration of the mean forces, *i-e*, by using formulas similar to Eqs. (6) and (7), with the constraint imposed on the centroid coordinate ξ instead of r. Similarly to the classical case, a series of simulation involving 15 values of ξ were performed for 4 selected values of R ($R=2.6$, 2.65, 2.7, and 2.8 Å). The full surface was then fitted by cubic spline interpolation. The same study was carried out for D instead of H, in order to evaluate the kinetic isotope effects. There are a number of interesting technical issues in all these calculations; they will be more carefully developed in a forthcoming publication.[59]

Sections of $\bar{W}(\xi,R)$ at two different values of R are presented in Figs. 9(a)–9(b). It can be seen that the surface incorporates the solvent stabilization effects, and also

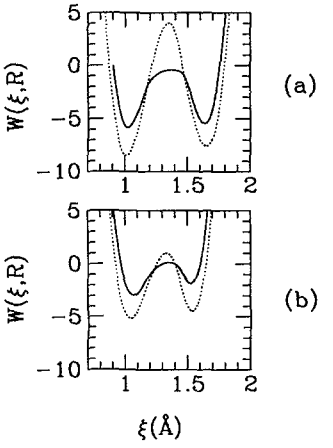

FIG. 9. Free energy along the centroid coordinate for two values of R: (a) $R=2.7$ Å; (b) $R=2.6$ Å. The classical free energy is shown for comparison (dashed line).

the main quantum contributions correcting the classical answer, the zero-point-energy (ZPE) corrections in the wells and a tunneling correction at the barrier.[26] The two latter contributions result in a substantial decrease of the free energy barrier with respect to the classical surface (3 kcal/mole at $R=2.6$ Å and 7 kcal/mole at $R=2.7$ Å).

Once $\bar{W}(\xi,R)$ is known, it is a simple matter to determine the QTST rate constant from Eqs. (39) and (40). Again, it is instructive to decompose the overall rate constant into its different R contributions in the following form:

$$k_Q^{\mathrm{TST}}=\int_0^{+\infty}dR\,g_A(R)\cdot k_Q^{\mathrm{TST}}(R), \tag{41}$$

where $g_A(R)$ is the distribution function of R in the reactant region, defined by $\xi<\xi^{\ddagger}(R)$. k_Q^{TST} is compared to the equivalent curve-crossing quantity in Fig. 10. The overall agreement is quite satisfactory and brings us some confidence regarding the validity of the two calculations, which are based on two independent numerical routes. The results obtained by the two methods are identical within the numerical error bars for $R\geqslant 2.65$ Å, *i-e*, in the nonadiabatic region of the reaction. A discrepancy appears in the adiabatic region: We find $k_Q^{\mathrm{TST}}/k_{\mathrm{LZ}}^{\mathrm{TST}}\simeq 2.5$ at $R=2.6$ Å. The same trend is recovered when looking at the integrated rate constants for the systems (I)–(III) of Sec. II. See Table III. The agreement decreases when going from the nonadiabatic system (I) to the adiabatic system (III). The relative difference in the apparent activation energies are found to be of 3%, 4%, and 15% for system (I)–(III), respectively (see Table III for a proper definition). For the latter system, modeling a fully adiabatic situation, the difference is beyond the error margins: The results of the two theories differ in a significant fashion (we find $k_Q^{\mathrm{TST}}/k_{\mathrm{LZ}}^{\mathrm{TST}}\simeq 2$). We believe that, in this case, the computation of the transmission coefficients κ_{LZ} and κ_Q would be necessary to possibly reconcile the curve-crossing and path-integral calculations. From our results, we expect $\kappa_Q>\kappa_{\mathrm{LZ}}$, which would favor the conclusion that, in the adia-

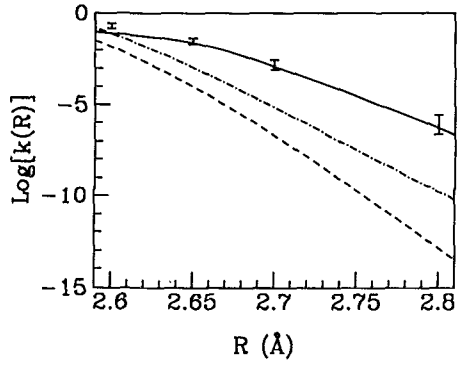

FIG. 10. Comparison of the R-dependent rate constant obtained by the different methods described in the text. The solid line is the curve-crossing rate of Fig. 8. The bars indicate the path-integral results obtained at different values of R, and the associated uncertainties. The dashed line is the classical answer corrected by ZPE effects. The dotted–dashed line incorporates the parabolic barrier tunneling factor of Eq. (45).

batic limit, thinking of the reaction in terms of a *solvent* coordinate as ΔE represents a better choice than a description connected to the proton coordinate itself (at least, if one accepts the definition of the "best reaction coordinate" as the one minimizing the transmission coefficient. Other criteria, as for example computational convenience, may also be important).

V. COMPARISON TO "CORRECTED" CLASSICAL THEORIES

It is interesting to estimate the tunneling contribution to the proton-transfer rate constant by comparing the results obtained previously to those coming from a "corrected" classical theory, in which a zero-point-energy (ZPE) correction and, possibly, a tunneling correction are added to the classical TST answer. This approach is often used to interpret experimental rates and isotope effects,[56] and deserves some critical comments in the present case.

In the latter approach, the rate constant may be expressed as

$$k_c = \int_0^\infty dR\, g_A(R) \cdot k_c(R), \tag{42}$$

$$k_c(R) = Z(R) \cdot T(R) \cdot \frac{\omega_A(R)}{2\pi} \exp(-\beta \Delta W^\ddagger(R)). \tag{43}$$

As before, $g_A(R)$ is the probability distribution function for R in the reactant state, $r < r_b(R)$. At each value of R, $\Delta W^\ddagger(R) = W(r_b(R),R) - W(r_A(R),R)$ is the barrier height for the *classical* free energy and $\omega_A(R)$ is the reactant proton frequency. The ZPE correction $Z(R)$ accounts for the quantization of the proton energy levels in the reactant well

$$Z(R) = \frac{2\sinh(\beta\hbar\omega_A(R)/2)}{\beta\hbar\omega_A(R)}. \tag{44}$$

The tunneling factor $T(R)$ is taken from the theory of Bell[60,61]

$$T(R) = \beta \int_{-\Delta W^\ddagger(R)}^\infty dE \frac{\exp(-\beta E)}{1+\exp(-2\pi E/\hbar\bar{\omega}_b(R))}. \tag{45}$$

$\bar{\omega}_b(R)$ is here an effective parabolic barrier frequency, which is related to the barrier width and the barrier height by[60]

$$\bar{\omega}_b(R) = a(R)^{-1}\sqrt{\frac{2\Delta W^\ddagger(R)}{m}}, \tag{46}$$

with $a(R) = r_b(R) - r_A(R)$. We note that for our model, we are always in the limit $u(R) = 2\pi/(\beta\hbar\bar{\omega}_b) < 1$, so that the high temperature expression $T(R) = u(R)/\sin(u(R))$ does not hold; the full integral formula (45) is needed then.

It can be seen in Fig. 10 that the rate constant obtained by incorporating the ZPE correction alone [$T(R) = 1$ in Eq. (43)] is always lower than the curve-crossing and path-integral results. The relative difference between the curves of Fig. 8 provides an estimation of the tunneling contribution to the rate. This contribution is considerable in the nonadiabatic regime [$k_{LZ}/k_c \simeq k_Q/k_c \simeq 10^3$ for system (I)] and still important in the adiabatic regime [$k_{LZ}/k_c \simeq k_Q/k_c \simeq 10^2$ for system (III); see Table III]. The incorporation of the parabolic barrier tunneling factor $T(R)$ reduces the discrepancy to $k_{LZ}/k_c \simeq 200$ for system (I) and $k_{LZ}/k_c \simeq 10$ for system (III); it is clearly unable to describe the tunneling effect properly. We think that the whole procedure is missing an important feature of the process, namely, the modulation of the proton tunneling by the fluctuations of the polar solvent. This feature is included in an explicit way in the activation free energy of Eq. (34), and in an implicit way in the path-integral formula, Eq. (40).

VI. CONCLUDING REMARKS

We have presented in this paper a realistic molecular model for describing OH–N proton-transfer reactions in polar, aprotic solvents. We have computed the rate constant by two different methods which are in reasonable agreement, and have shown how the rate and the associated isotopic substitution effect are dependent on the strength of the H bond along which the proton-transfer occurs.

Proton-transfer reactions along weak OH–N bonds, represented by the model (I) of our study, are in the nonadiabatic limit. They are characterized by an important tunneling contribution and a correspondingly large isotope effect (KIE > 100). There is also an important solvent activation energy, since the proton-transfer involves an extensive charge reorganization. This limit is most likely applicable to intramolecular transfers in which acceptor and donor atoms are maintained far apart.

On the other hand, proton transfers along strong H bonds, similar to the case (III) of our study are induced by the dynamics of the solvent rather than the tunneling of the proton. The reaction is rather rapid then ($k > 10^9\ s^{-1}$) and the corresponding activation energy is contained mostly in

the solvent coordinates. The associated kinetic isotope effect is small (KIE$\sim$10). We believe that many proton transfers in intermolecular complexes belong to this class and that this property, rather than the general applicability of the Bell theory, might explain the small values of the generally measured isotope effects. Arguments in the same direction have been given elsewhere.[62]

On a methodological point of view, we have shown how a semiclassical curve-crossing strategy can be implemented to determine the rate constant. This determination is accomplished by the simulation of classical, rigid molecules, at very low computational cost. The results have been compared to those of a path-integral calculation. The overall agreement is indeed satisfactory, since the two methods seem to go on very different routes. (A theoretical connection exists of course, but it is only clear in the tunneling regime and for model Hamiltonians.[22,24] A unifying approach consists in choosing the centroid of the energy gap ΔE as the reaction coordinate of the path-integral formulation, instead of the Cartezian centroid.[7]) For the problem presented here, the centroid method is computationally much more demanding, since it requires to determine a free energy surface instead of simple charge-transfer quantities.[63] The situation could be reversed for problems involving the coupling of the proton to many anharmonic quantum modes. We believe that, in this case, the path-integral formulation would be more efficient.[64] The centroid simulations could be simplified by the trick of Ref. 21, i.e., by using classical trajectories and averaging subsequently over the free particle distribution, or also by using a microscopic influence-functional approach.[59]

Our final point of discussion is that the possibility of computing the quantum transmission coefficient of the path-integral theory at a simulation level is not clear yet, whereas several semiclassical methods are available in the curve-crossing perspective. This might be an important issue for the treatment of adiabatic reactions, since we have found that, in this limit, there is a discrepancy between the two approaches at a transition-state level, and dynamical prefactors should be properly accounted for. This will be a direction of future research.

ACKNOWLEDGMENTS

The simulations have been performed with the support of the scientific committee of the Centre de Calcul Vectoriel pour la Recherche (Palaiseau, France). It is a pleasure to thank J. T. Hynes and H. Ratajczak for fruitful discussions and G. Tarjus and Z. Latajka for their critical comments.

APPENDIX A: MARCUS RELATIONSHIP FOR OUTER-SPHERE CHARGE TRANSFERS

We consider an arbitrary charge transfer between two fixed charge configurations A and B. Let H_A and H_B be the corresponding diabatic Hamiltonians, including the interaction with the solvent coordinates $\mathbf{S}$; as in the text, $\Delta E(\mathbf{S}) = H_A - H_B$ is the solvent-dependent splitting and C the coupling. We define the diabatic free energy curves by

$$G_X(\Delta E) = -k_B T \times \ln\left[\int d\mathbf{S}\, e^{-\beta H_X}\delta(\Delta E(\mathbf{S})-\Delta E)/\int d\mathbf{S} e^{-\beta H_0}\right], \quad X=A,B. \tag{A1}$$

We take here the adiabatic ground state as a reference state, in order to match the diabatic and adiabatic descriptions. H_0 is given by a formula similar to that in Eq. (4). Defining $H_{\hat{\imath}} = \frac{1}{2}(H_A + H_B)$, we can express the diabatic free energies by using $H_{\hat{\imath}}$ as a reference Hamiltonian:

$$G_A(\Delta E) = k_B T \ln\frac{Q_0}{Q_{\hat{\imath}}} + \frac{\Delta E}{2} - k_B T \ln\langle\delta(\Delta E(\mathbf{S})-\Delta E)\rangle_{\hat{\imath}},$$

$$G_B(\Delta E) = k_B T \ln\frac{Q_0}{Q_{\hat{\imath}}} - \frac{\Delta E}{2} - k_B T \ln\langle\delta(\Delta E(\mathbf{S})-\Delta E)\rangle_{\hat{\imath}}, \tag{A2}$$

where $\langle\cdot\rangle_{\hat{\imath}}$ indicates an average performed with $H_{\hat{\imath}}$, and Q_0, $Q_{\hat{\imath}}$ are the partition functions corresponding to H_0 and $H_{\hat{\imath}}$, respectively. By making use of the Gaussian property (i) of Sec. III A, we can put G_A and G_B in the form,

$$G_A(\Delta E) = G_A^0 + \frac{1}{2}\frac{k_B T}{\langle\delta\Delta E^2\rangle_{\hat{\imath}}}(\Delta E - \langle\Delta E\rangle_A)^2,$$

$$G_B(\Delta E) = G_A^0 + \frac{1}{2}\frac{k_B T}{\langle\delta\Delta E^2\rangle_{\hat{\imath}}}(\Delta E - \langle\Delta E\rangle_B)^2 - \langle\Delta E\rangle_{\hat{\imath}}, \tag{A3}$$

with

$$\langle\Delta E\rangle_A = \langle\Delta E\rangle_{\hat{\imath}} - \frac{\langle\delta\Delta E^2\rangle_{\hat{\imath}}}{2k_B T},$$

$$\langle\Delta E\rangle_B = \langle\Delta E\rangle_{\hat{\imath}} + \frac{\langle\delta\Delta E^2\rangle_{\hat{\imath}}}{2k_B T},$$

$$G_A^0 = \frac{\langle\Delta E\rangle_{\hat{\imath}}}{2} - \frac{\langle\delta\Delta E^2\rangle_{\hat{\imath}}}{8k_B T} + k_B T \ln\left[\frac{Q_0}{Q_{\hat{\imath}}}\right] + \frac{1}{2}k_B T \ln\left[2\pi\frac{\langle\delta\Delta E^2\rangle_{\hat{\imath}}}{k_B T}\right]. \tag{A4}$$

It can be easily checked that the two formulas in Eq. (A3) fulfill the exact relationship [see also Eq. (A2)]

$$G_A(\Delta E)=G_B(\Delta E)+\Delta E. \tag{A5}$$

Furthermore, the diabatic curves turn out to have equal curvature, a feature familiar to continuum dielectric theories. The reaction free energy ΔG and the solvent reorganization energy E_r are here defined in microscopic terms by

$$\Delta G=G_B(\langle\Delta E\rangle_B)-G_A(\langle\Delta E\rangle_A)=-\langle\Delta E\rangle_{\dot{I}}\,,$$
$$E_r=G_B(\langle\Delta E\rangle_A)-G_B(\langle\Delta E\rangle_B)=\frac{\langle\delta\Delta E^2\rangle_{\dot{I}}}{2k_BT}. \tag{A6}$$

Expressions similar to Eqs. (25) and (26), involving averages over the diabatic states (A) and (B) instead of $(\dot{I})$ can be easily derived from Eqs. (A4)–(A6). It can be verified also that the Marcus relationship between activation and free energies is fulfilled, i.e.,

$$G_A(0)-G_A(\langle\Delta E\rangle_A)=\Delta G^{\ddagger}=\frac{(\Delta G+E_r)^2}{4E_r}. \tag{A7}$$

APPENDIX B: EXPRESSION OF THE COUPLING $C(R,\Delta E)$

In the total Hamiltonian of our system, Eq. (4), the electrostatic interaction term V_c can be expanded around $\mathbf{R}_0$, the position of the center of the A-B bond, in the form,

$$V_c(r,R,\mathbf{S})=V_c(\mathbf{S})-\mu(r,R)\cdot\mathscr{E}(\mathbf{S})+\cdots. \tag{B1}$$

$\mu(r,R)$ represents the dipole of the complex at fixed geometry and $\mathscr{E}(\mathbf{S})$ is the electric field along the A-B bond at $\mathbf{R}_0$.

We could verify that, for our model, the dipolar interactions are largely dominant, so that the expansion in Eq. (B1) can be limited to the first two terms (See, e.g., the results in Table II; this property leads to interesting simplifications which we will exploit in a forthcoming publication.) In this case, the diabatic energy splitting ΔE and the coupling C may be written as

$$\Delta E=(\mu_B-\mu_A)\mathscr{E}+(E_A^g-E_B^g),$$
$$C=\frac{2(H_{AB}^g-\mu_{AB}\mathscr{E})-S_{AB}[E_A^g+E_B^g-(\mu_A+\mu_B)\mathscr{E}]}{2(1-S_{AB}^2)}, \tag{B2}$$

where $E_{A,B}^g=\langle\Psi_{A,B}|H_g|\Psi_{A,B}\rangle$ and $H_{AB}^g=\langle\Psi_A|H_g|\Psi_B\rangle$ denote the gas-phase, intrinsic matrix elements, and μ_A, μ_B, μ_{AB} are the corresponding dipole elements. The expression (27) of the coupling C is therefore recovered with

$$C_0(R)=(1-S_{AB}^2)^{-1}\left(H_{AB}^g-\frac{(\mu_{AB}+S_{AB}\mu_B)E_A^g-(\mu_{AB}+S_{AB}\mu_A)E_B^g}{\mu_A-\mu_B}\right),$$
$$C_1(R)=(1-S_{AB}^2)^{-1}\left(\frac{\mu_{AB}-\frac{1}{2}S_{AB}(\mu_A+\mu_B)}{\mu_A-\mu_B}\right). \tag{B3}$$

[1] H. Ratajczak and W. J. Orville-Thomas, in *Molecular Interactions*, edited by H. Ratajczak and W. J. Orville-Thomas (Wiley, New York, 1980), Vol. 1.
[2] Th. Zeegers-Huyskens and P. Huskens, in *Molecular Interactions*, edited by H. Ratajczak and W. J. Orville-Thomas (Wiley, New York, 1980), Vol. 2.
[3] H. Ratajczak, J. Phys. Chem. **76**, 3000 and 3991 (1972).
[4] H. Ratajczak and W. H. Orville-Thomas, J. Chem. Phys. **58**, 991 (1973).
[5] A. Warshel and R. M. Weiss, J. Am. Chem. Soc. **102**, 6218 (1980).
[6] A. Warshel, *Computer Modeling of Chemical Reactions in Proteins and Solutions* (Wiley, New York, 1991).
[7] A. Warshel and Z. T. Chu, J. Chem. Phys. **93**, 4003 (1990).
[8] J. Juanós i Timoneda and J. T. Hynes, J. Phys. Chem. **95**, 10431 (1991).
[9] M. Ilczyszyn, H. Ratajczak, and J. A. Ladd, Chem. Phys. Lett. **153**, 385 (1988); J. Mol. Struct. **198**, 499 (1989).
[10] H. Ratajczak, in *Electron and Proton Transfer Processes in Chemistry and Biology*, edited by A. Müller, H. Ratajczak, W. Junge, and E. Diemann (Elsevier, Amsterdam, 1992).
[11] D. Borgis and J. T. Hynes, Chem. Phys. Lett. **162**, 19 (1989).
[12] D. Borgis and J. T. Hynes, J. Chem. Phys. **94**, 3619 (1991).
[13] D. Borgis, in *Electron and Proton Transfer Processes in Chemistry and Biology*, edited by A. Müller, H. Ratajczak, W. Junge, and E. Diemann (Elsevier, Amsterdam, 1992).
[14] D. Borgis, G. Tarjus, and H. Azzouz, J. Phys. Chem. **96**, 3188 (1992); J. Chem. Phys. **97**, 1390 (1992).
[15] D. Laria, G. Ciccotti, M. Ferrario, and R. Kapral, J. Chem. Phys. **97**, 378 (1992).
[16] K. Haug, G. Wahnström, and H. Metiu, J. Chem. Phys. **92**, 2083 (1990).
[17] T. N. Truong, J. A. McCammon, D. J. Kouri, and D. K. Hoffman, J. Chem. Phys. **96**, 8136 (1992).
[18] P. Bala, B. Leysyng, T. N. Truong, and J. A. McCammon, in *Molecular Aspects of Biotechnology: Computational Models and Theories*, edited by J. Bertran (Kluwer Academic, The Netherlands, 1992).
[19] J. C. Tully, J. Chem. Phys. **93**, 1061 (1990).
[20] F. A. Webster, P. J. Rossky, and R. A. Friessner, Comp. Phys. Commun. **63**, 494 (1991).
[21] J. K. Hwang, Z. T. Chu, A. Yadav, and A. Warshel, J. Phys. Chem. **95**, 8445 (1991).
[22] M. Gillan, J. Phys. C **20**, 3621 (1987); Phys. Rev. Lett. **58**, 563 (1987).
[23] G. A. Voth, D. Chandler, and W. H. Miller, J. Phys. Chem. **93**, 7009 (1989); J. Chem. Phys. **91**, 7749 (1989).
[24] G. A. Voth and E. V. Gorman, J. Chem. Phys. **94**, 7342 (1990).
[25] D. Li and G. A. Voth, J. Phys. Chem. **95**, 10425 (1991).
[26] J. Lobaugh and G. A. Voth, Chem. Phys. Lett. (in press).
[27] N. Makri and W. H. Miller, J. Chem. Phys. **87**, 5781 (1987); **91**, 4026 (1989).
[28] E. Bosch, M. Moreno, and J. M. Lluch, Chem. Phys. **159**, 99 (1992).
[29] For a useful classification of proton transfers along H bonds, see P. Schuster, W. Jakubetz, W. Meyer, and B. M. Rode, in *Chemical and Biochemical Reactivity*, edited by E. D. Bergman and B. Pullman (Jerusalem, 1974). See also Ref. 13.
[30] D. Borgis and J. T. Hynes (in preparation).
[31] E. R. Lippincott and R. Schroeder, J. Chem. Phys. **23**, 1099 and 1131 (1955); with respect to the original potential, we have omitted the direct attractive interaction between A and B. This term brings only minor modifications to the strong attractive contribution already contained in Eq. (2).
[32] S. Bratos, H. Ratajczak, and P. Viot, in *Hydrogen-Bonded Liquids*, edited by J. C. Dore and J. Texeira (Kluwer Academic, Netherlands, 1991).
[33] The charge switching function is taken independent of R for simplicity. The total charge distribution of the complex is still function of R through the position of the partial charges on A and B.
[34] B. Bigot, B. J. Costa-Cabral, and J. L. Rivail, J. Chem. Phys. **83**, 3083 (1985).
[35] A. Warshel, J. Phys. Chem. **86**, 2218 (1982).
[36] W. P. Keirstead, K. R. Wilson, and J. T. Hynes, J. Chem. Phys. **95**, 5256 (1991).
[37] J. K. Hwang, C. Creighton, D. Whitney, and A. Warshel, J. Chem. Phys. **89**, 859 (1988); J. Am. Chem. Soc. **110**, 5297 (1988).

[38] L. I. Trakhtenberg, V. L. Klochikin, and S. Ya. Pshezhetsky, Chem. Phys. **69**, 121 (1982).
[39] R. I. Cukier and M. Morillo, J. Chem. Phys. **92**, 4833 (1990).
[40] A. Suárez and R. Silbey, J. Chem. Phys. **94**, 4809 (1991).
[41] J. K. Hwang and A. Warshel, J. Am. Chem. Soc. **109**, 715 (1987).
[42] G. King and A. Warshel, J. Chem. Phys. **93**, 8682 (1990).
[43] E. A. Carter and J. T. Hynes, J. Phys. Chem. **93**, 2184 (1989); J. Chem. Phys. **94**, 5961 (1991).
[44] D. A. Zichi, G. Ciccotti, J. T Hynes, and M. Ferrario, J. Phys. Chem. **93**, 6261 (1989).
[45] M. D. Newton and N. Sutin, Ann. Rev. Phys. Chem. **35**, 437 (1984).
[46] R. A. Kuharski, J. S. Bader, D. Chandler, M. Sprik, and M. L. Klein, J. Chem. Phys. **89**, 3248 (1988).
[47] See, e.g., E. E Nikitin, *Theory of Elementary Atomic and Molecular Processes in Gases* (Clarendon, Oxford, 1974).
[48] E. Carter, G. Ciccotti, M. Ferrario, and R. Kapral, Chem. Phys. Lett. **156**, 472 (1989).
[49] E. Paci, G. Ciccotti, M. Ferrario, and R. Kapral, Chem. Phys. Lett. **176**, 581 (1991).
[50] M. P. Allen and D. J. Tildesley, *Computer Simulation of Liquids* (Clarendon, Oxford, 1987).
[51] M. Tachiya, J. Phys. Chem. **93**, 7050 (1989).
[52] This expression of the solvent activation energy is not strictly correct in the adiabatic limit: In this case, $\Delta E=0$ does not correspond exactly to the maximum of the ground-state adiabatic curve. The distinction is not important however for proton-transfer reactions, since the coupling remains always small, even in the adiabatic limit ($C<1$ kcal/mol). On the other hand, this effect is, in principle, corrected by the dynamical prefactor κ_{LZ} in the exact rate formula (18).
[53] E. D. German, A. M. Kuznetsov, and R. R. Dogonadze, J. Chem. Soc. Faraday Trans. II **76**, 1128 (1980).
[54] J. Ulstrup, *Charge Transfer Processes in Condensed Media* (Springer, Berlin, 1979).
[55] The value of α is a little bit too large with respect to previous estimations ($\alpha \simeq 30$ Å^{-1}, see, e.g., Ref. 11). This appears as a drawback of the Lippincott–Schroeder functional adopted in this work, which seems to overestimate the variation of the coupling with R, as well as the stiffness of the potential along R. The important point, however, is that the basic physical trends are reproduced correctly.
[56] E. F. Caldin and V. Gold, *Proton Transfer Reactions* (Chapman and Hall, London, 1975).
[57] R. P. Bell, *The Tunnel Effect in Chemistry* (Chapman and Hall, London, 1980).
[58] See, e.g., D. Chandler, in *Liquids, Freezing and Glass Transition*, edited by D. Levesque, J. P Hansen, and J. Zinn-Justin (Elsevier, Amsterdam, 1990).
[59] H. Azzouz and D. Borgis (in preparation).
[60] R. P. Bell, Trans. Faraday Soc. **55**, 1 (1959).
[61] R. P. Bell, J. Chem. Soc. Faraday Trans. II **76**, 954 (1980).
[62] E. D. German and A. Kuznetsov, J. Chem. Soc. Faraday Trans. II **77**, 2203 (1981).
[63] In the curve-crossing perspective, the knowledge of the classical free energy surface leads to a convenient definition of the diabatic states, but it is not a necessary input.
[64] J. S. Bader, R. A. Kuharski, and D. Chandler, J. Chem. Phys. **93**, 230 (1990).